Misra Vasubandhu (Orcid ID: 0000-0002-1345-6280)

Integrated Kinetic Energy of Atlantic Tropical Cyclones in a Global Ocean Surface Wind Analysis

Sean Buchanan[1, 2, 3],Vasubandhu Misra[1, 2, 3, #], and Amit Bhardwaj[2,3]

[1]Department of Earth, Ocean and Atmospheric Science, Florida State University, Tallahassee, Florida, U. S. A.

[2]Center for Ocean-Atmospheric Prediction Studies, Florida State University, Tallahassee, Florida, U. S. A.

[3]Florida Climate Institute, Florida State University, Tallahassee, Florida, U. S. A.

Corresponding Author email: vmisra@fsu.edu

Abstract

The Integrated Kinetic Energy (IKE) of a Tropical Cyclone (TC), a volume integration of the surface winds around the center of the TC is computed from a comprehensive surface wind (NASA's Cross-Calibrated Multi-platform [CCMP]) analysis available over the global oceans to verify against IKE from wind radii estimates of extended best track data maintained by NOAA for the North Atlantic TCs. It is shown that CCMP surface wind analysis severely underestimates IKE largely from not resolving hurricane force winds for majority of the Atlantic TCs, under sampling short lived and small sized TCs. The seasonal cycle of the North Atlantic TC IKE also verifies poorly in the CCMP analysis. In this paper we introduce proxy IKE (PIKE) based on the kinetic energy of the winds at the Radius Of the last Closed Isobar (ROCI), which shows promise for a wide range of TC sizes including the smaller sized TCs unresolved in the CCMP dataset.

Keywords: Tropical cyclones, Integrated Kinetic Energy, Reanalysis,

2

1 Introduction

Atmospheric and oceanographic reanalysis are major accomplishments achieved by the scientific community that have opened doors of understanding the complexities of climate and its variations over the years. In particular, Tropical Cyclone (TC) studies have utilized such advancements to understand their structure, dynamics and influence on climate variability. For instance, Hart et al. (2007) studied the local memory of atmospheric and oceanic variability after TC passage using the 40-Year European Centre for Medium-Range Weather Forecasts (ECMWF) Re-Analysis (ERA-40); Sriver and Huber (2007) examined the average oceanic heat transport by TCs; Hart (2011) examined the influence of TC activity on poleward heat transport through changes to the meridional heat flux. However, the constant concern of coarse grid resolution, limitations of the physics and dynamics of the data assimilation models, the shortcomings of data assimilation methodologies, observational errors and scarcity of observations representing TCs in the reanalysis have always persisted. For example, the limitations of atmospheric reanalysis in representing the intensity and location of the TCs are highlighted in Schenkel and Hart (2012) and Zick and Matyas (2015). Schenkel and Hart (2012) found that majority of the reanalysis datasets poorly resolve TC location and intensity. LaRow (2013) used the Center for Ocean-Atmospheric Prediction Studies (COAPS) Land-Atmosphere Regional Reanalysis for the Southeast (CLARReS10; Stefanova et al. 2012) at 10km grid interval to study landfalling TCs for the years 1979-

3

2000 and found that near-surface winds were inadequately resolved when compared to the observed data. Similarly, Jourdain et al. (2014) investigated oceanic responses to TC surface winds by extracting wind data from ECMWF operational analysis and ERA-Interim reanalysis. They found that TC surface winds, on average, grossly underestimated intensity parameters causing misrepresentation of vertical mixing and Ekman pumping in the cold wake of the TC passage in the global eddy-permitting ocean reanalyses that were utilized.

Our motivation in this research is to examine the usability of a well-known sea-surface wind analysis dataset like the National Aeronautics and Space Administration's (NASA's) funded Cross-Calibrated Multi-Platform Ocean Surface Wind Vector L3.0 First-Look Analysis (hereafter referred CCMP; Atlas et al. 2011) for TC application studies. For this study, we have used the metric of Integrated Kinetic Energy (IKE; Powell and Reinhold 2007) to examine the fidelity of TC features in CCMP. IKE is the volume integral of the square of the surface winds from the Radii of Maximum Winds (RMW) to gale-force strength (17 ms^{-1} or 34-kt; 1 kt H 0.5ms^{-1}) (Powell and Reinhold 2007; Misra et al. 2013). IKE, emphasizes on the spatial distribution of the surface winds around the TC unlike other metrics that overemphasize the peak sustained winds measured at a particular point and completely neglect the size of the TC (Franklin et al. 2003; Nolan et al. 2014). For example, accumulated cyclone energy (Bell et a. 2000) causes overestimation of seasonal TC activity because it uses only the point measurement

4

of peak sustained winds (Yu et al 2009; Yu and Chiu 2012). Furthermore, Powell and Reinhold (2007) suggest that IKE represents the destructive potential of a TC far better than other metrics as the kinetic energy of the surface wind scales with wind loads on structures and also scales with the surface wind stress over ocean surface that force storm surge. The objective of this study is to validate IKE of the Atlantic TCs in the CCMP analysis and assess its usability for TC IKE diagnostic studies.

A brief discussion on the data sets used in this study are provided in Section 2. We present our methodologies to perform our validation of IKE from CCMP in Section 3. Section 4 discusses the results with final conclusions in Section 5.

2 Datasets

a) *The extended best track dataset*

The Colorado State University Extended Best Track (EBT) dataset (Demuth et al. 2006) provide wind radii data for TCs in the North Atlantic (NA) basin for the 1988-2015 period. From 1988 to 2003, the EBT wind radii were copied from the operational estimates found in the Automated Tropical Cyclone Forecast (ATCF) data files. In 2004, the wind radii became a formal best-tracked quantity in HURDAT2. Since 2004, the EBT wind radii use these values. Similarly, RMW in EBT is also from the operational estimates of the a-decks in the automated tropical cyclone forecast system. But unlike the

5

intensity and position parameters in HURDAT2 the RMW through the entire period are simply operational estimates and are not subject to post season best track analysis (Landsea and Franklin 2013). In fact, Vigh et al. (2012) have pointed to significant inconsistencies between aircraft measurements of RMW and outer wind radii with those reported in EBT. Furthermore, Landsea and Franklin (2013) indicate that these wind radii estimates have an uncertainty range of 25% to 52% depending on its operational data source (which includes ship and buoy, aircraft, satellite based estimates, and operational analyses). Nonetheless, Knaff et al. (2016) and Dolling et al. (2016) have indicated that these wind radii estimates are reasonable to use for method development studies despite their prevailing uncertainties. Furthermore, the EBT wind radii data has now been extended for a limited time period (2001-present) to the east Pacific basin (http://rammb.cira.colostate.edu/research/tropical_cyclones/tc_extended_best_track_data set/). We will explore the IKE analysis of TCs in other tropical ocean basins in a future study. But for this study we will be confined to the NA basin.

b) CCMP winds

The CCMP analysis provides sea-surface winds at a height of 10 meters around the globe with the exception of the Arctic Ocean (Atlas et al. 2011). It has been widely used for a number of ocean related studies (Zheng et al. 2016; Oey et al. 2013) including TC studies (Zhang et al. 2013; Vukicevic et al. 2014; Pei et al. 2015). The CCMP surface

6

wind   analysis   version   1.1

(https://podaac.jpl.nasa.gov/dataset/CCMP_MEASURES_ATLAS_L4_OW_L3_0_WIN

D_VECTORS_FLK) is available at 0.25° grid spacing at 6-hourly intervals from 1987-

2011. This analysis has been developed using the Variational Analysis Method (VAM;

Hoffman et al. 2003) that combines in situ, remotely sensed observations (microwave

radiometers and scatterometers; e.g., WindSat and QuikScat respectively), and first guess

estimate from analyses (ECMWF reanalysis [ERA-40] was used for 1987-1998 period

and ECMWF operational analysis thereafter). Satellite retrieved surface winds from the

Remote Sensing Systems (RSS) are derived after inter-calibrating the radiometers at a

brightness temperature level to within 0.2ºC by using a refined sea-surface emissivity

model and a radiative transfer function (Atlas et al. 2011). This results in these wind

retrievals being highly consistent across the different microwave radiometer platforms

(e.g. SSM/I, SSMIS, AMSR, TMI, WindSat and GMI). In addition, both the

scatterometer and radiometer data is validated against the ocean moored buoys that

exhibit agreements to within 0.8ms^{-1}. The VAM using the ERA-40 analysis as the

background wind field assimilates the RSS instrument data with the moored ocean buoy

measurements to produce the CCMP surface wind analysis referenced at a height of 10

meters above the surface.

3 Methodology

7

The definition of (total) IKE following Powell and Reinhold's (2007) is:

$$IKE = \frac{1}{2}\int_h \int_{r_{MW}}^{r_{XX}} \int_0^{2\pi} \rho r V^2 d\alpha dr dz - - - - - - - (1)$$

where, Á is a constant value for air density, which is taken to be 1.15 kgm^{-3}, V is the surface wind speed, and the integration is a volume integral of the surface winds for a thickness of 1 meter (h) between the observed radii of maximum wind (RMW; r_{MW}) and radii of gale force winds (r_{xx}; 17 ms^{-1} or 34 knots [kt]), and α is the sector angle. Misra et al. (2013) developed a historical IKE dataset for the NA TCs using EBT for the years 1990-2011, which is now extended to 2014. Because the data available from EBT is not gridded but available for the four quadrants of the TC, Misra et al. (2013) have suggested a detailed algorithm to compute IKE from such discrete data (Table 1). This dataset will be used as the validation dataset when comparing CCMP-IKE values. We separated the total IKE (equation 1) from EBT into 3 components (34-, 50-, and 64-kt IKE) for further comparison. In other words, we partitioned total IKE into IKE$_{34-50}$, IKE$_{50-64}$, and IKE$_{64-RMW}$ discretely as the sum of the square of the winds between 34-kt and 50-kt, 50-kt and 64-kt, and 64-kt and RMW respectively from both EBT and CCMP datasets (following equation 2a). It should be noted that the EBT considers the asymmetries in the surface wind structure of the TC by providing estimates of wind radii in the primary intercardinal directional (Northeast, Southeast, Southwest and Northwest) quadrants of the TC at each fix and further we follow the algorithm provided in Table 1 following

8

Misra et al. (2013). However, CCMP being a gridded analysis (albeit at 0.25° spatial resolution) provides an opportunity for a more accurate account of TC surface wind asymmetries than EBT.

It is well known that the size of the TC has a stronger bearing on IKE than the peak sustained wind speeds (Powell and Reinhold 2007; Musgrave et al. 2012; Misra et al. 2013; Kozar and Misra 2014). Therefore, the size (or spatial extent) of the 34-kt winds for TCs play a significant role in the total IKE than the comparatively smaller spatial extent of the 50-kt and 64-kt winds (Kozar and Misra 2014). We therefore also computed separately IKE_{34-50}, IKE_{50-64}, and IKE_{64-RMW} from CCMP analysis to validate with corresponding IKE derived from EBT data. These were computed as:

$$IKE_{r_{XX}-r_{YY}} = \frac{1}{2} \int_h \int_{r_{YY}}^{r_{XX}} \int_{\theta_{CCMP;EBT}} \rho r V^2 d\alpha dr dz - - - - - - - (2a)$$

where, r_{xx} and r_{yy} refers to the radii for one of the four wind speeds (34-kt, 50-kt, 64-kt, V_{MAX}), and the differing limits of integration of d± owing to the difference in the discretization of the two datasets (CCMP and EBT) would therefore follow as:

$$\theta_{CCMP} = 0 < \alpha < 2\pi - - - - - - - (2b)$$

$$\theta_{EBT} = \begin{cases} 0 < \alpha < \frac{\pi}{2}, \text{as } \theta_1 \text{ in the first quadrant} \\ \frac{\pi}{2} < \alpha < \pi, \text{ as } \theta_2 \text{ in second quadrant} \\ \pi < \alpha < \frac{3\pi}{2}, \text{as } \theta_3 \text{ in third quadrant} \\ \frac{3\pi}{2} < \alpha < 2\pi, \text{as } \theta_4 \text{ in fourth quadrant} \end{cases} - - - - - - (2c)$$

9

For example, EBT IKE computed between 34-kt and 50-kt winds will be computed as:

IKE_{34-50}

$$= \frac{1}{2}\int_h \left\{ \int_{r_{50}}^{r_{34}} \int_{\theta_1} rV^2 d\alpha dr \right.$$

$$+ \int_{r_{50}}^{r_{34}} \int_{\theta_2} rV^2 d\alpha dr + \int_{r_{50}}^{r_{34}} \int_{\theta_3} rV^2 d\alpha dr + \left. \int_{r_{50}}^{r_{34}} \int_{\theta_4} rV^2 d\alpha dr \right\} dz - - - - (3a)$$

It may be noted that the above sectoral area integrals within the curly brackets in equation 3a are discretely computed following the algorithm outlined in Table 1. However, in the gridded dataset of CCMP, IKE computed for example, between 34-kt and 50-kt winds will be:

$$IKE_{34-50} = \frac{1}{2}\int_h \int_{r_{50}}^{r_{34}} \int_0^{2\pi} \rho rV^2 d\alpha dr dz - - - - - - (3b)$$

This difference in methodology of computing IKE from a gridded analysis like CCMP (using equation 3b) and from dataset like EBT (equation 3a) is apparent.

However, we quickly found that CCMP poorly resolves 50-kt and 64-kt winds in TCs of the NA basin. In fact, of the 1414 and 979 fixes of TCs that had 50-kt and 64-kt winds in the EBT data (for the period 2004-2011) there were only 289 and 218 fixes in the corresponding CCMP analysis respectively. Therefore, given such poor capture and small sample size of the TC wind structure at high wind speeds, we have limited our discussion of the verification results to only the IKE_{34-50} of TCs in the CCMP analysis.

Table 2 clearly shows that the 34-kt radii variation explains more variance of the total IKE than the radii of the other two specified wind regimes in the EBT data. It may be noted that all correlation values in Table 2 pass the 5% significance level according to t-test. Furthermore, the choice of the time period (exclusively using best-track years vs non-best track years of EBT) chosen has the least impact on this relationship for all three wind speed ranges (Table 2).

In order to understand the methodological differences in the diagnosis of IKE between EBT and CCMP IKE, we computed IKE in CCMP using both equations 3a and b. It may be noted that we diagnosed the maximum radial extent of 34-kt winds in each of the 4 quadrants before using equation 3a for the CCMP dataset. Fig. 1 shows the difference in IKE estimates from the two methodologies (equations 3a and b) for all TC fixes in the CCMP dataset that resolved 34-kt winds or higher in at least one of the quadrants. It is clearly seen from this figure that equation 3a overestimates IKE relative to equation 3b. For the sake of consistency in verifying with EBT IKE we choose to use equation 3a to compute CCMP IKE even though the use of equation 3b would provide a more representative estimate of IKE for a given TC fix in a gridded analysis like the CCMP dataset.

4 Results

a) Validation of CCMP surface wind analysis

The EBT dataset contains 2353, 6-hourly time fixes of TCs with IKE_{34-50} values for the years 2004-2011. However, CCMP only resolved 514 fixes out of the aforementioned 6-hourly time fixes with 34-kt wind radii. Atlas et al. (2011) clearly indicate that all microwave sensors used in the CCMP analysis are sensitive to rain with increasing rain rate associated with decreased accuracy. Further, data gaps of satellite retrieved winds can also result in such poor validation. A scatter plot between CCMP's resolved IKE_{34-50} against EBT's IKE_{34-50} (Fig. 2a) and EBT's total IKE (Fig. 2b) displays the fidelity of the CCMP wind structure of NA TCs. It may be noted that in Figs. 2a and b there are only 514 TC fixes resolved by CCMP analysis. The explained variance of CCMP's IKE_{34-50} on the corresponding EBT's IKE_{34-50} ($R^2 = 31\%$) in Fig. 2a is similar to that for total IKE from EBT ($R^2 = 32\%$; Fig. 2b). The comparable values of R^2 value between Figs. 2a and b suggest yet again that the radii of the 34-kt wind is critical for total IKE in the EBT dataset. The majority of the points in the scatter plot of Fig. 2a lie above the diagonal line (y=x) suggesting that there is a systematic underestimation of IKE from CCMP relative to EBT. There is however a significant minority of fixes (with IKE ranging up to about 100TJ) for which CCMP overestimates IKE relative to the EBT dataset. Similarly, Fig. 2b also shows that IKE_{34-50} from CCMP underestimates the total IKE from EBT for a majority of TC fixes with IKE <100TJ. The relatively large RMSE values in Figs. 2a and b reemphasize the bias in the CCMP TC wind structure.

12

The climatological seasonal cycle of the number of TCs and IKE_{34-50} computed over the period of 2004-2011 are shown in Figs. 3a and b respectively. The number of TCs in EBT dataset in Fig. 3a (2279 over all seasons) correspond to TCs which had 34-kt wind reported at least in one quadrant in at least one 6-hourly fix over the lifetime of the TC. Similarly, the number of TCs in the CCMP dataset in Fig. 3a (505 over all seasons) are those in which the 34-kt wind radii is resolved in at least one 6-hourly fix over the lifetime of the TC. Fig. 3a clearly shows that the CCMP systematically underestimates the number of fixes and the number of TCs throughout the NA season. In the months of August, September and October the differences in the count of both the TCs and the fixes between CCMP and EBT datasets are the largest (Fig. 3a). In a related study, Misra et al. (2013) indicate that these are the months when TC's in the NA have the longest lifespans and acquire their largest size. Coincidentally, we also observe that the largest bias in CCMP IKE appear in August, September and October (Fig. 3b). The IKE bias in the CCMP dataset is so severe that even its seasonal cycle is not well represented. For example, CCMP shows a seasonal peak in July followed by the next maximum in November contrary to the EBT dataset. We also compared the seasonal cycle of IKE for the same fixes in both CCMP and EBT datasets (i.e., for the 505 fixes of CCMP; not shown) and found the differences to be qualitatively very similar to Fig. 3b. This indicates that at least the bias in the seasonal phase of IKE in the CCMP analysis in Fig. 3b is largely from the bias in the TC size and its wind structure.

13

We also computed the track density expressed as the number of TCs per 2°x2° cell with non-zero IKE_{34-50} separately from both EBT and CCMP analysis (Fig. 4). It may be noted that in Fig. 4 TCs that stayed within one cell for multiple 6-hourly time fixes were counted as many times as they appeared in the cell. In examining Figs. 4a-c, a number of features can be noted: i) The overall track density across NA Ocean is generally far less in CCMP relative to EBT, ii) the track density differences are comparatively less in the Gulf of Mexico and near the Gulf coastal regions than those in central and eastern Atlantic Ocean (Caribbean Sea), and iii) the largest differences in track density are observed in the deep tropical Atlantic in the Main Development Region (MDR; 10°-20°N, 80°-20°W) and in the subtropical latitudes including the Atlantic coast. The bias over the MDR suggests that CCMP has difficulty in resolving TC's at time of genesis when they are small in size and are also potentially short lived. There are however other reasons for the differences between Figs. 4a and b. For instance, there is a higher frequency of TC fixes in the open ocean in the EBT data than near the coasts, which then leads to the likelihood of more differences from CCMP dataset over open oceans because of the sample size differences. Another reason is that in the open ocean CCMP analysis relies more heavily on remotely sensed wind that is contaminated by rain clouds of the TC and therefore results in less coverage of TC winds by CCMP analysis (Atlas et al. 2011).

14

b) The proxy IKE in CCMP analysis

Given the relatively poor validation of the TC wind structure in the CCMP analysis especially for the smaller sized TCs, we resort to the development of a proxy IKE (PIKE), which is defined as the contour integral of the product of the square of the winds at the Radius Of the last Closed Isobar (ROCI) and the radius of the last closed isobar (r_{ROCI}). The concept of PIKE is fundamentally motivated by the fact that IKE is more dependent on the size of the TC than its maximum sustained wind speed. Mathematically, PIKE may be expressed as:

$$\text{PIKE} = \int_h \oint_{r_{ROCI}}^{r_{ROCI}} \rho r_{ROCI} V_{ROCI}^2 \, dc \, dz - - - - - - - - - - - - (4)$$

Equation 4 suggests that PIKE is the kinetic energy based on winds at ROCI (V_{ROCI}) that is integrated along the contour of r_{ROCI}. Further motivation to develop PIKE is the increased likelihood of resolving the winds at ROCI in CCMP analysis because of its weaker wind speeds and larger size than radii of winds stronger or equal to tropical storm strength. In addition, the relative distance of ROCI from the very active areas of convection around the center of the TC and along the surrounding rain bands would make the diagnosis of the winds less susceptible to contamination from precipitating clouds in the CCMP analysis. Furthermore, PIKE from CCMP analysis provides the likelihood for better verification with IKE from EBT data because IKE is far more sensitive to the size of the TC than wind speed (Powell and Reinhold 2007; Misra et al. 2013) and ROCI is a good measure of the size of the TC (Carrasco et al. 2014).

15

Very importantly we are able to compute PIKE for all 2353 TC fixes in the EBT dataset for which IKE was computed. This is because PIKE is designed to capture the variations of IKE based on winds at ROCI and does not require TC in CCMP to acquire tropical storm strength winds or higher. In comparison, it may be noted that the CCMP analysis resolved only 21.8%, 20%, and 22% of the TC fixes with 34-kt, 50-kt, and 64-kt wind radii TC's relative to EBT data respectively. The seasonal cycle of PIKE is slightly improved over that of CCMP (Fig. 3b) with at least the seasonal peak appearing in September as in EBT dataset. However, PIKE underestimates EBT IKE in every month of the season significantly. This bias is expected given that PIKE is purely based on winds at ROCI which would be much weaker than the tropical storm strength or higher wind speeds. The largest bias of PIKE appear in September and November while the smallest bias is displayed in June followed by August (Fig. 3b). This suggests that PIKE displays greater benefit over CCMP IKE for small sized TCs that typically are observed in early part of the Atlantic hurricane season. The bias in PIKE begins to increase substantially in the months when large sized TCs with associated asymmetries, are more prevalent during the seasonal peak and towards the end of the season. The asymmetries cause distortion of the ROCI from a symmetric single value provided by EBT for each TC fix. As a result, PIKE is bound to develop a bias for such TCs.

A display of the distribution (boxplot) of the winds at ROCI (Fig. 5) indicates that the median wind at ROCI – for all 8 years of study – is around 9.2ms^{-1} with maximum

16

winds near gale-force strength in some of the years (e.g. 2004, 2009, 2011). These comparatively strong winds at ROCI are usually on account of the asymmetric features from the extra-tropical transition of a relatively large sized TC (Kimball and Mulekar 2004; Evans and Hart 2003). Furthermore, it should be noted that ROCI is affected by the translation speed of the TC, which makes its estimate fairly difficult and uncertain (Merill 1984; Chu et al. 2002; Cocks and Gray 2002). In addition, the pressure of the last closed isobar in EBT takes on discrete integer values of 1hPa and ROCI could vary a fair amount over that interval. Therefore, the wind speeds at ROCI could have substantial variance as indicated in Fig. 5. Finally, some subjectivity exists in estimates of ROCI especially when last closed isobar is distorted (Cocks and Gray 2002).

The scatter between IKE from EBT and PIKE computed from CCMP wind analysis at ROCI is shown in Fig. 6a for all (2353) TC fixes between 2004-2011, which indicates a correlation of 0.67 (or $R^2 = 0.45$) and RMSE value of 35.10 TJ. In comparison, the conventional IKE computed from the CCMP wind analysis for all 2353 fixes of EBT dataset displayed a correlation of 0.56 (or $R^2=0.32$) and RMSE value of 40.46TJ (Fig. 2b). The improvement of PIKE is further corroborated in Fig. 6b, which shows the scatter of PIKE and IKE from EBT exclusively for TC fixes with tropical storm strength winds that were not resolved by CCMP analysis. Here the correlation between PIKE and IKE is 0.71 ($R^2=0.50$) and RMSE is 33.41 TJ.

A composite track density of TC fixes falling at or below the 10th and at or above the 90th percentile of absolute difference between IKE and PIKE (|IKE – PIKE|) to represent the most closely and poorly validated estimates of IKE from PIKE are shown in Figs. 7a and b with their difference in Fig. 7c respectively. The value for the 10th (90th) percentile in absolute difference is 0.92 TJ (55.67 TJ). In examining Figs. 7a-c, we see some overlap in the geographical location of the TC fixes whose PIKE value most poorly and closely validate EBT IKE. There is however a subtle difference with more recurving TCs and TCs with a northerly track (likely undergoing extratropical transition) validating more poorly (Fig. 7a) than the relatively zonally tracking TCs of the deep tropics (Fig. 7b). One of the explanations for this difference is the higher values of IKE for larger sized extra-tropical cyclones (Misra et al. 2013) that increases the likelihood increased magnitude of errors in the estimates of IKE from PIKE relative to EBT derived IKE values. Furthermore, increasing asymmetries in the wind structure as TCs undergo extra-tropical transition (Evans and Hart 2003) result in reducing the validity of using a symmetric estimate for ROCI obtained from EBT. In addition, estimating ROCI where the last closed isobar is distorted (which is likely to be the case for TC undergoing extra-tropical transition) in itself is uncertain. These factors are likely to increase the discrepancy between PIKE from CCMP and IKE from EBT especially for such asymmetric TCs.

We also show the scatter of the EBT IKE with PIKE and CCMP IKE for the fixes for which PIKE verified poorly (fixes at 90th percentile or above for the difference between PIKE and EBT IKE; Fig. 8) and reasonably (fixes at 10th percentile or below for the difference between PIKE and EBT IKE; Fig. 9). In both these instances, we clearly see that PIKE outperforms CCMP IKE. It is quite clear from all of this analysis that PIKE is a good alternative to IKE in the CCMP dataset. In comparing Figs. 8 and 9 it is clear that PIKE verifies better with EBT IKE in instances of TC with smaller IKE.

5 Conclusions

The aim of the paper was to examine the fidelity of the TC-IKE over several hurricane seasons of the Tropical North Atlantic (NA) in the Cross-Calibrated Multi-Platform Ocean Surface Wind Vector L3.0 First-Look (CCMP) analysis. We used the Extended Best Track (EBT) data for validation. IKE relies on the structure of specified surface wind regimes, which makes it a reliable metric to estimate potential damage from storm surge and wind load on structures. Because IKE is not dependent on a transient feature like the peak sustained wind speed but volume integrates the surface wind from the center of the TC out to 34-kt wind speed, it has considerable inertia and therefore has the potential to be simulated or predicted better than other TC metrics (Kozar and Misra 2014; Kozar et al. 2016). It should be noted however that the observed wind radii estimates from EBT have considerable uncertainty, which makes any validation exercise

19

of IKE challenging. However, it is imperative to pursue these studies despite the limitations of observations given the growing recognition of the importance of TC size and IKE on the potential impacts of landfalling TCs.

The CCMP analysis was found to barely resolve 34-kt winds in the majority of TCs let alone winds at 50-kt and 64-kt wind reported in EBT. We therefore computed IKE_{34-50} from the CCMP wind analysis, which only resolved 21.8% of comparable fixes in EBT. It was found that IKE_{34-50} from CCMP analysis was found to explain about 30% of the variance of the total IKE in the EBT data for the NA basin for the resolved TC fixes in the CCMP analysis. The CCMP analysis was also found to particularly have issues of IKE bias in TCs that were small in size and short in lifespan. In many such cases, CCMP failed to resolve the TC fixes. Large TCs with long lifespans are invariably resolved in the CCMP irrespective of their location (either in the open ocean or near the coast). But the areal coverage of gale-force winds for large TCs were also underestimated in the CCMP analysis relative to the EBT dataset giving rise to large errors in the estimates of IKE. The climatological seasonal cycle of IKE_{34-50} for the NA TCs are also very poorly validated in the CCMP winds. The seasonal peak of IKE in CCMP appears in July which is contrary to the EBT dataset that shows seasonal peak in September. Furthermore, CCMP also grossly underestimate total IKE and the number of fixes relative to EBT data.

20

A proxy IKE (PIKE) based on the volume integration of the square of the winds at the Radius of the last Closed Isobar (ROCI) is introduced. PIKE from CCMP analysis shows promise in validating with EBT IKE. PIKE shows significant improvement over IKE from CCMP for a broad range of TC sizes. PIKE however displays larger bias for northward tracking NA TC's. This may be a result of the increasing influence of wind asymmetries of larger sized TCs that is not reasonably well represented in PIKE owing to symmetric single values of ROCI for each TC fix.

Acknowledgments

References

Atlas, R., R. N. Hoffman, J. Ardizzone, S. M. Leidner, J. C. Jusem, D. K. Smith, D. Gombos, 2011: A cross-calibrated, multiplatform ocean surface wind velocity product for meteorological and oceanographic applications. *Bull. Amer. Meteor. Soc.*, **92**, 157-174, doi: 10.1175/2010BAMS2946.1.

Bell, G. D., M. S. Halpert, V. E. Kousky, M. E. Gelman, C. F. Ropelewski, A. V. Douglas, and R. C. Schnell, 2000: Climate assessment for 1999. *Bulletin of the American Meteorological Society* **81**:6, S1-S50.

Chu, J.-H., C. R. Sampson, A. S. Levine, and E. Fukada, 2002: The Joint Typhoon Warning Center tropical cyclone best-tracks, 1945–2000. Ref. NRL/MR/7540-02, 16.

Cocks, S. B., and W. M. Gray, 2002: Variability of the outer wind profiles of western North Pacific typhoons: Classifications and techniques for analysis and forecasting. Mon. Wea. Rev., **130**:8, 1989–2005.

Carrasco, C., C. Landsea, and Y. Lin, 2014: The influence of tropical cyclone size on its intensification. Wea. Forecasting, 29, 582-590.

22

Evans, J. L., and R. E. Hart, 2003: Objective indicators of the life cycle evolution of extratropical transition for atlantic tropical cyclones. *Mon. Wea. Rev.*, **131**, 909-925.

Demuth, J., M. DeMaria, and J.A. Knaff, 2006: Improvement of advanced microwave sounder unit tropical cyclone intensity and size estimation algorithms. *J. Appl. Meteor.*, **45**, 1573-1581.

Dolling, Klaus, Elizabeth A. Ritchie, and J. Scott Tyo, 2016: The Use of the Deviation Angle Variance Technique on Geostationary Satellite Imagery to Estimate Tropical Cyclone Size Parameters. *Weather and Forecasting,* 31 (5), 1625-1642.

Franklin, J. L., M. L. Black, and K. Valde, 2003: GPS dropwindsonde profiles in hurricanes and their operational implications. Wea. Forecasting, 18, 32–44, doi:10.1175/1520-0434(2003)018,0032: GDWPIH.2.0.CO;2.

Gray, W. M., 1968: Global view of the origins of tropical disturbances and storms. *Mon. Wea. Rev.*, **96**, 669–700.

Hart, R.E., 2011: An inverse relationship between aggregate tropical cyclone activity and subsequent winter climate. *Geo. Res. Lett.*, **38**, L01705, doi:10.1029/2010GL045612.

Hart, R., R. Maue, and M. Watson, 2007: Estimating the atmospheric and SST memory of tropical cyclones through MPI anomaly evolution. *Mon. Wea. Rev.*, **135**, 3990-4005.

Hoffman, R. N., S. M. Leidner, J. M. Henderson, R. Atlas, J. V. Ardizzone, and S. C. Bloom, 2003: A two-dimensional variational analysis method for NSCAT ambiguity removal: Methodology, sensitivity, and tuning. J. Atmos. Oceanic Technol., 20, 585–605

Jourdain, N. C., B. Barnier, N. Ferry, J. Vialard, C. E. Menkes, M. Lengaigne, and L. Parent, 2014: Tropical cyclones in two atmospheric (re)analyses and their response in two oceanic reanalyses. *Ocean Modelling,* **73**, 108-122.

Kimball, S., and M. Mulekar, 2004: A 15-Year Climatology of North Atlantic Tropical Cyclones, Part 1: Size Parameters. *Journal of Climate*, **17**, 3555-3575.

Knaff, J. A., C. J. Slocum, K. D. Musgrave, C. R. Sampson, and B. R. Strahl, 2016: Using routinely available information to estimate tropical cyclone wind structure. M*on. Wea. Rev.*, 144(4), 1233-1247. DOI: http://dx.doi.org/10.1175/MWR-D-15-0267.1

Kozar, M. E., and V. Misra, 2014: Statistical Prediction of Integrated Kinetic Energy in North Atlantic Tropical Cyclones. *Mon. Wea. Rev .*, **142**, 4646-4657.

Kozar, M. E., V. Misra, and M. Powell, 2016: Hindcasts of Integrated Kinetic Energy in Atlantic tropical cyclones: A neural network prediction scheme. Mon. Wea. Rev. In press. Doi:http://dx.doi.org/10.1175/MWR-D-16-00301.1.

Landsea, C.W., and J.L. Franklin, 2013: Atlantic Hurricane Database Uncertainty and Presentation of a New Database Format. Mon. Wea. Rev., 141, 3576-3592.

LaRow, T., 2013: An analysis of tropical cyclones impacting the Southeast United States from a regional reanalysis. *Regional Environmental Change* 13:S1, 35-43.

Martin, J. D., and W. M. Gray, 1993: Tropical cyclone observation with and without aircraft reconnaissance. *Wea. and Forecasting*, **8**, 519-532.

Merrill, R. T., 1984: A comparison of large and small tropical cyclones. Mon. Wea. Rev., **112**:7, 1408–1418, doi:10.1175/1520-0493

Misra V., S. DiNapoli, and M. Powell, 2013: The Track Integrated Kinetic Energy of Atlantic 615 Tropical Cyclones. *Mon. Wea. Rev.,* 141:7, 2383-2389.

Musgrave K.D.*,* R. K.Taft*,* J. L.Vigh*,* B. D.McNoldy*, and* W. H.Schubert*,* 2012: Time evolution of the intensity and size of tropical cyclones, *J. Adv. Model. Earth Syst.,* 4*,* M08001.

Nolan, D., J. A. Zhang, E. W. Uhlhorn, 2014: On the limits of estimating maximum wind speeds in hurricanes. *Mon. Wea. Rev*., 142, 2814-2832.

Oey, L. –Y., M.-C. Chang, Y.-L. Chang, Y.-C. Lin, F.-H. Xu, 2013: Decadal warming of coastal China Seas and coupling with winter monsoon and currents. *Geophysical Research Letters* **40**:23, 6288-6292.

Pei, Y.H., RongHua Zhang, and DaKe Chen, 2015: Upper ocean response to tropical cyclone wind forcing: A case study of typhoon Rammasun (2008). *Science China Earth Sciences* **58**:9, 1623-1632.

Powell, M.D., and T. A. Reinhold, 2007: Tropical Cyclone Destructive Potential by Integrated 627 Kinetic Energy. *Bull. Amer. Meteor. Soc.*, **88**, 513–526.

Schenkel, B. and R. E. Hart, 2012: An examination of tropical cyclone position and intensity differences within reanalysis datasets. *J. Climate*, MERRA Special Collection, **25**, 3453-3475. doi: 10.1175/2011JCLI4208.1.

Sriver, R., and M. Huber, 2007: Observational evidence for an ocean heat pump induced by tropical cyclones. *Nature*, **447**, 577–580.

Stefanova, L., V. Misra, S. Chan, M. Griffin, J. O'Brien, and T. Smith, 2012: A proxy for high-resolution regional reanalysis for the Southeast United States: assessment of

precipitation variability in dynamically downscaled reanalysis. *Clim Dyn.,* **38**:2449–2466.

Vigh, J. L., J. A. Knaff, and W. H. Schubert, 2012: A climatology of hurricane eye formation. *Mon. Wea. Rev.,* 140, 1405–1426, doi:10.1175/MWR-D-11-00108.1

Vukicevic, T., E. Uhlhorn, P. Reasor, B. Klotz, 2014: A Novel Multiscale Intensity Metric for Evaluation of Tropical Cyclone Intensity Forecasts. *Journal of the Atmospheric Sciences* **71**:4, 1292-1304.

Yu, J.-Y., and P.-G. Chiu, 2012: Contrasting various metrics for measuring tropical cyclone activity. *Terr. Atmos. Oceanic Sci.*, **23**, 303–316.

Yu, J. –Y., C. Chou, and P.-G. Chiu, 2009: A revised accumulated cyclone energy index. *Geophys. Res. Lett.*, **36**, L14710, doi:10.1029/2009GL039254.

Zhang, R. –H., Yuhua Pei, and Dake Chen, 2013: Remote effects of tropical cyclone wind forcing over the western Pacific on the eastern equatorial ocean. *Advances in Atmospheric Sciences* **30**:6, 1507-1525.

Zheng, C. W., Jing Pan, and Chong Yin Li, 2016: Global oceanic wind speed trends. *Ocean & Coastal Management* **129**, 15-24.

27

Zick, S. E., C. J. Matyas, 2015: Tropical cyclones in the North American Regional Reanalysis: An assessment of spatial biases in location, intensity, and structure. *Journal of Geophysical Research: Atmospheres* **120:5**, 1651-1669.

Table 1: Algorithm to compute IKE from EBT wind radii data (Adapted from Misra et al. 2013)

Annulus contribution to IKE	Condition	Mean Wind (kt)	Area
IKE_{34-50}	$R_{50} > 0$	40	$1/4\ \pi(R_{34}{}^2 - R_{50}{}^2)$
	No R_{50}, $V_{MAX} > 50$, $R_{34} > RMW$	40	$1/4\ \pi(R_{34}{}^2 - (0.75RMW)^2)$
	No R_{50}, $V_{MAX} < 50$, $R_{34} > RMW$	$1/4\ V_{MAX} + 3/4\ (34)$	$1/4\ \pi(R_{34}{}^2 - (0.75RMW)^2)$
	No R_{26}, $RMW = R_{34}$	34	$1/4\ \pi(R_{34}{}^2 - (0.5R_{34})^2)$
IKE_{50-64}	$R_{64} > 0$	27.75	$1/4\ \pi(R_{50}{}^2 - R_{64}{}^2)$
	no R_{64}, $V_{MS} > 64$, $R_{50} > RMW$	27.75	$1/4\ \pi(R_{50}{}^2 - (0.75RMW)^2)$
	no R_{64}, $V_{MAX} < 64$, $R_{50} > RMW$	$.25\ V_{MAX} + .75\ (50)$	$1/4\ \pi(R_{50}{}^2 - (0.75RMW)^2)$
	no R_{64}, $R_{50} <= RMW$	26	$1/4\ \pi[R_{50}{}^2 - (.5R_{50})^2]$
$IKE_{>64}$	Max R_{64} Quadrant, $R_{64} > RMW$	$.25V_{MAX} + .75(64)$	$1/4\ \pi(R_{64}{}^2 - (0.75RMW)^2)$
	Max R_{64} Quadrant, $R_{64} = RMW$	$.25V_{MAX} + .75(64)$	$1/4\ \pi(R_{64}{}^2 - (.75\ R_{64})^2)$
	$R_{64} < RMW$	$.1V_{MAX} + .9(64)$	$1/4\ \pi(R_{64}{}^2 - (.75\ R_{64})^2)$
	Not max R_{64} Quadrant $RMW = R_{64}$	$.1V_{MAX} + .9(64)$	$1/4\ \pi(R_{64}{}^2 - (0.75RMW)^2)$

V_{max}: Maximum sustained wind speed; RMW: Radius of maximum wind speed

29

Table 2: The correlation of Integrated Kinetic Energy (IKE) with wind radii from Extended Best Track (EBT) data (Demuth et al. 2006) for three different time periods.

	All years (1990-2014)	Non-best track years (1990-2003)	Best track years (2004-2014)
34-kt radii	0.91	0.92	0.93
50-kt radii	0.83	0.84	0.84
64-kt radii	0.68	0.65	0.73
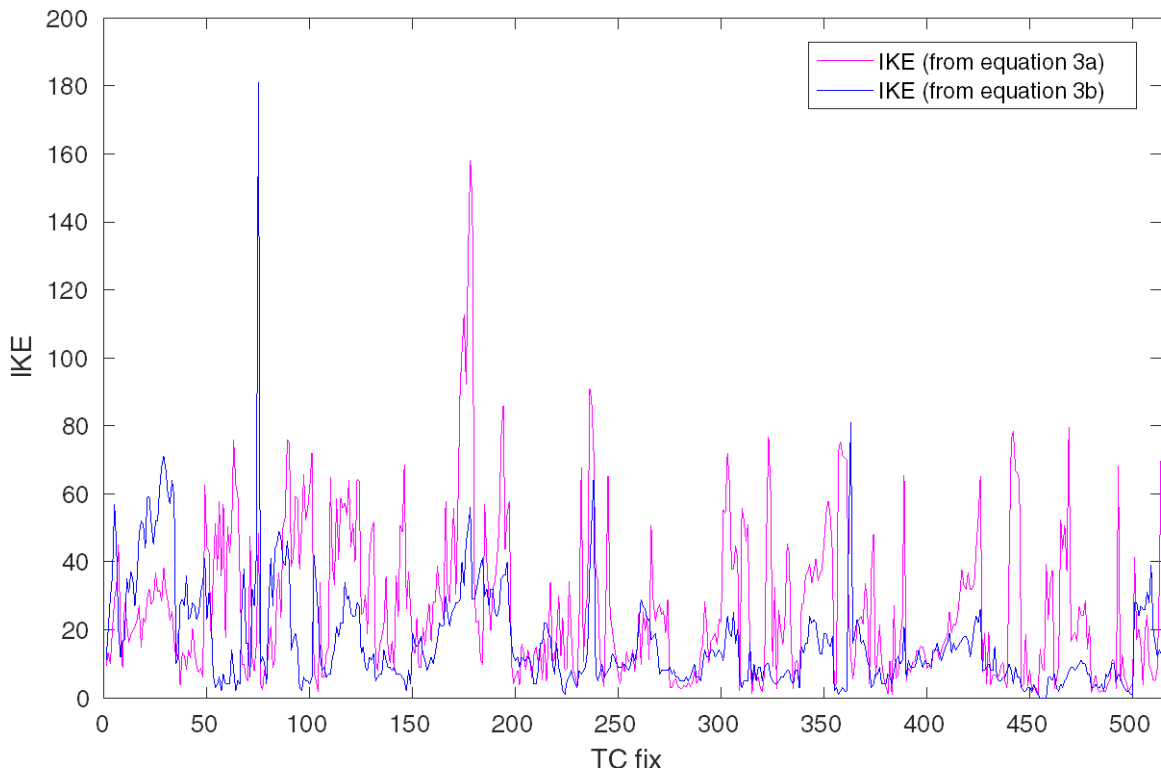
Figure 1: IKE (in TJ) computed from equations 3a and b from CCMP datasets for all

514 TC fixes in which 34-kt or greater wind speed was resolved.

A. EBT IKE$_{34-50}$ vs Resolved CCMP IKE$_{34-50}$

$R^2 = 0.31$

RMSE = 35.20

EBT IKE$_{34-50}$

CCMP IKE$_{34-50}$

B. EBT IKE vs Resolved CCMP IKE$_{34-50}$

$R^2 = 0.32$

RMSE = 40.46

EBT IKE

CCMP IKE$_{34-50}$
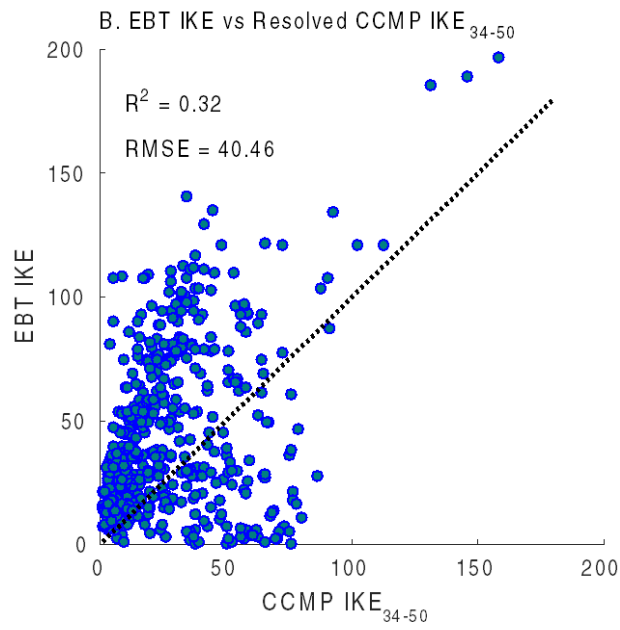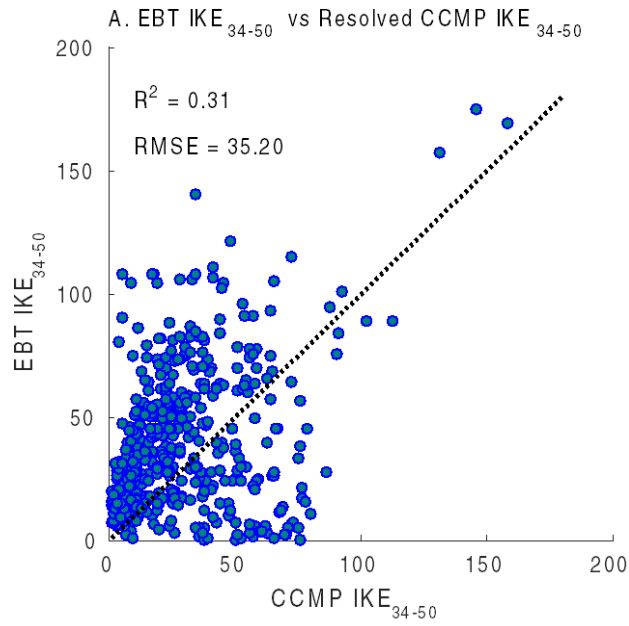
Figure 2: Scatter of IKE (in Terra Joules; TJ) from Cross-Calibrated Multi-Platform (CCMP) surface wind analysis (Atlas et al. 2011) with corresponding EBT data (Demuth et al. 2006) for Atlantic TCs from 2004-2011. Top (a) scatter shows the spread of EBT IKE_{34-50} versus the CCMP IKE_{34-50} (equation 3a in text). (b) Scatter of EBT total IKE (equation 1 in text) versus CCMP IKE_{34-50}. The units of RMSE is TJ. The dotted black line is y=x line.

33

	June	July	August	September	October	November
EBT IKE 34-50	59	258	579	999	271	113
CCMP IKE 34-50	5	41	123	200	89	47
EBT TCs	6	13	34	44	20	7
CCMP TCs	4	7	15	26	6	5
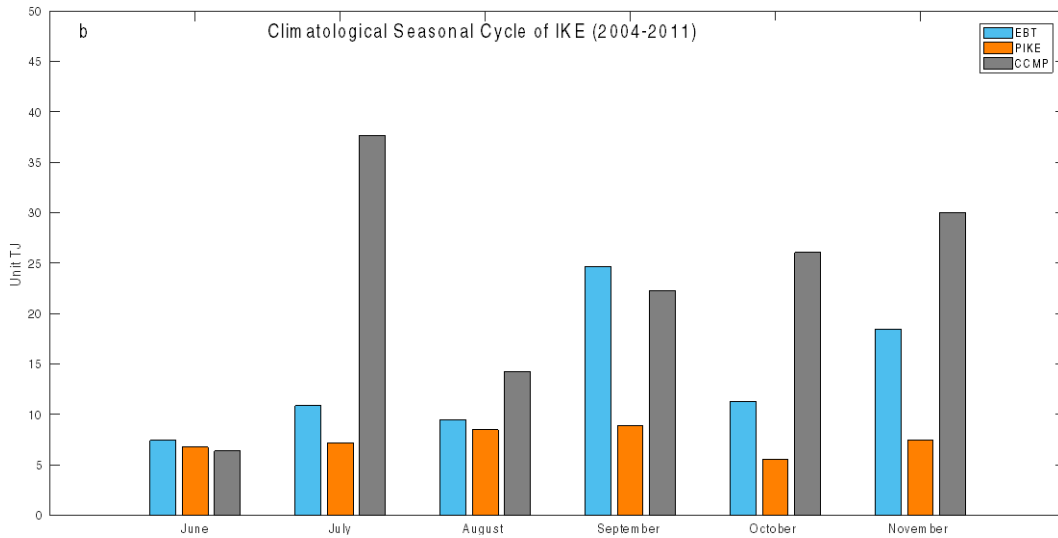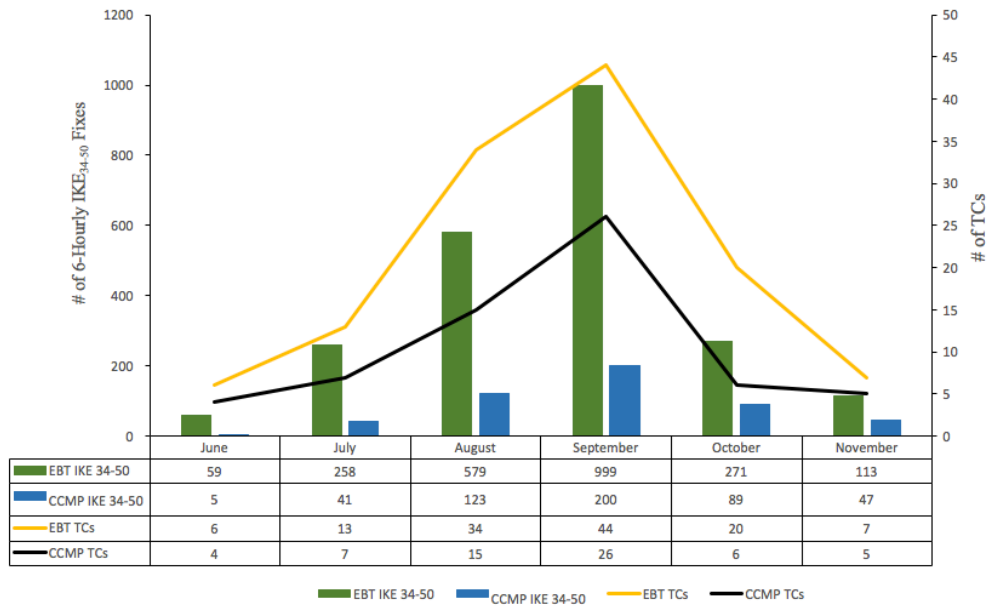
Figure 3: a) Climatological seasonal cycle of the number of fixes used in computing IKE from EBT (green bar) and CCMP (blue bar) datasets. These fixes reported with 34-kt wind at least in one quadrant in the EBT or over one grid point in the CCMP datasets.

34

Similarly, the number of TCs in the EBT (yellow line) and the corresponding number of resolved TCs in the CCMP (black line) are also shown. The numerical values of the number of fixes (in the first two rows) and number of TCs (in the bottom two rows) from EBT and CCMP datasets are indicated in the embedded table. b) Climatological seasonal cycle of IKE (TJ) from EBT (blue bar), CCMP (grey bar) and ProxyIKE (TJ; PIKE; orange bar) computed from CCMP dataset. Since the sample sizes in CCMP and EBT dataset are so disparate, we used the median IKE values for each month to reduce the influence of the different sample size on the climatological seasonal cycle of IKE.
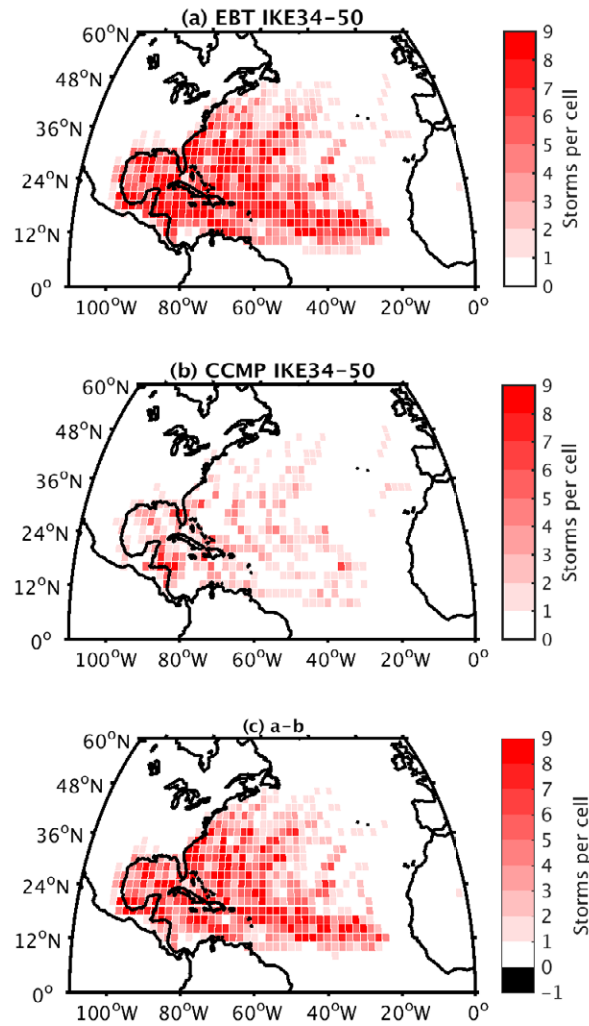
Figure 4: The composite track density (number of TCs based on non-zero values of IKE_{34-50} per 2°x2° cell) plot of North Atlantic TCs for the years 2004-2011 from a) EBT, b) CCMP, and c) a-b. The grid cells are of equal area, normalized by the cosine of latitude.
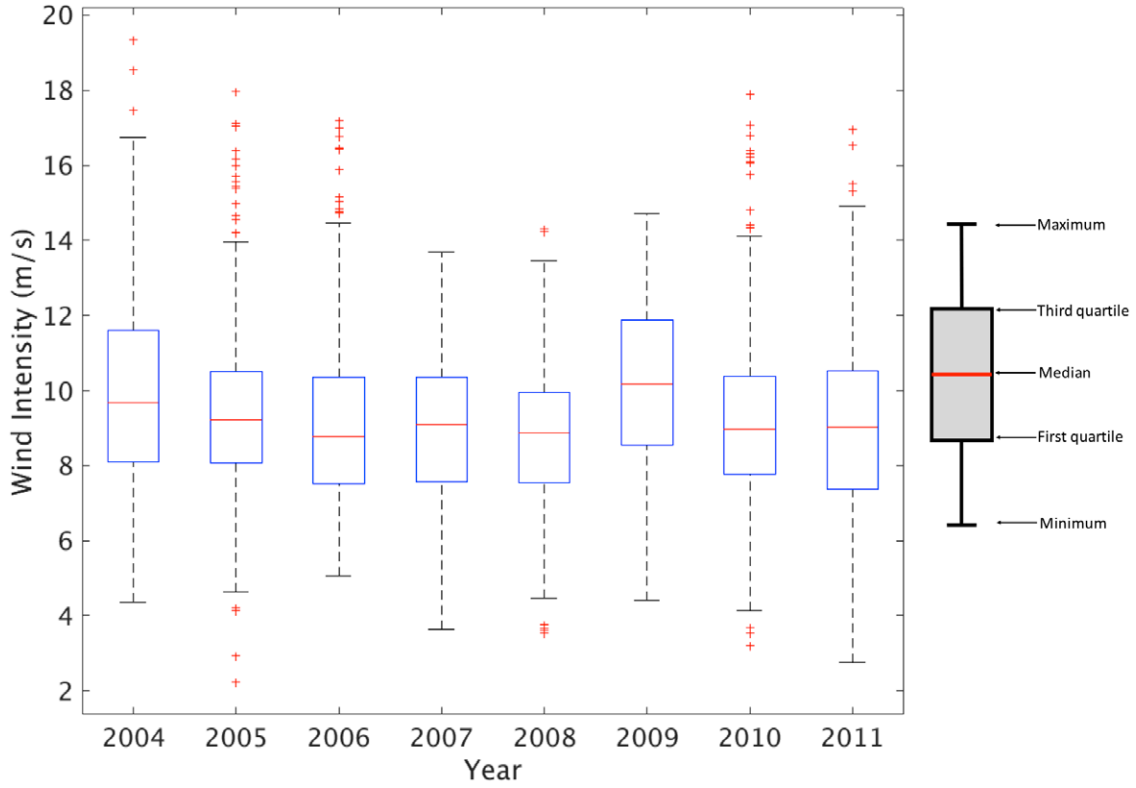
Figure 5: Boxplot depicting the distribution of the magnitude of the wind speed at ROCI in CCMP wind analysis. The index for the boxplot is shown in the far top right. The outliers are shown by the red + signs.
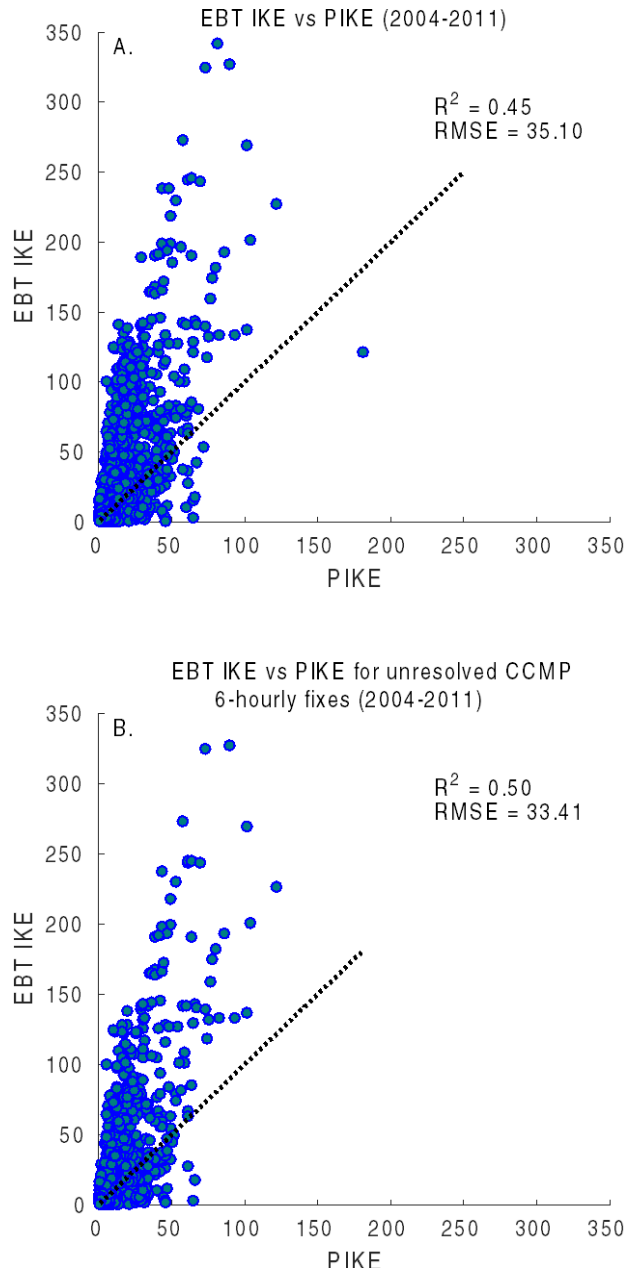
Figure 6: The scatter between PIKE (equation 4; TJ) based on surface winds from CCMP winds and total EBT IKE (equation 1; TJ) for a) all fixes in the EBT data and b)

for TC fixes with at least tropical storm strength winds in EBT data that is unresolved in CCMP analysis. The dotted black line in both panels is y=x line.
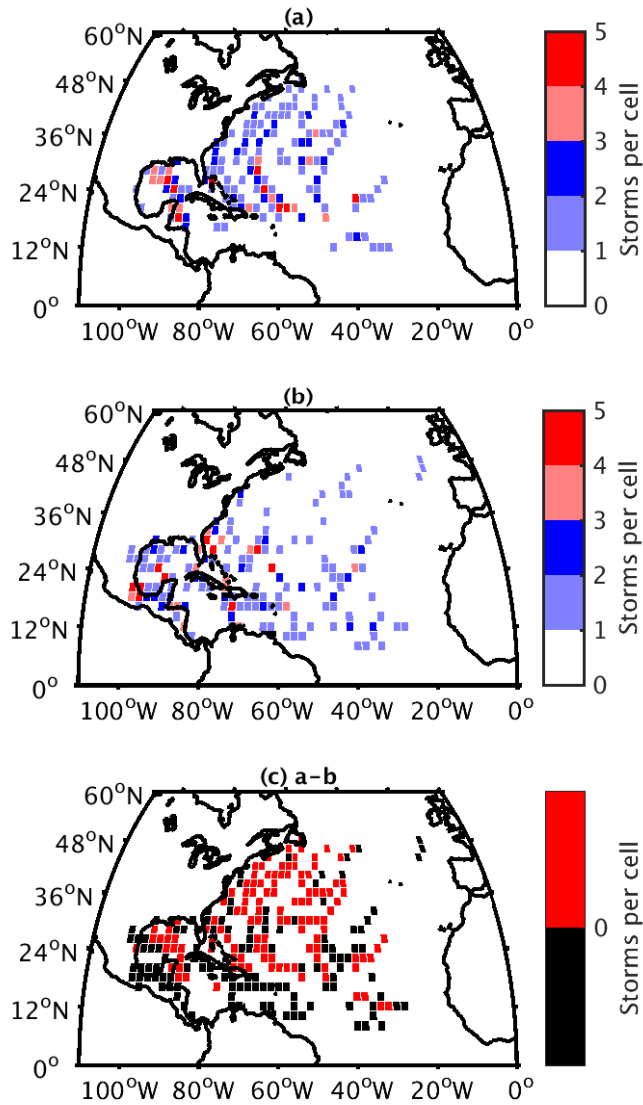
Figure 7: The composite track density (number of TCs per 2°x2° cell) plot of TCs for which the PIKE from CCMP validates most a) poorly, b) closely (see text for

explanation), and c) a-b with corresponding IKE of TCs from EBT for the 2353 fixes between the years 2004-2011. The grid cells are of equal area, normalized by the cosine of latitude.

41
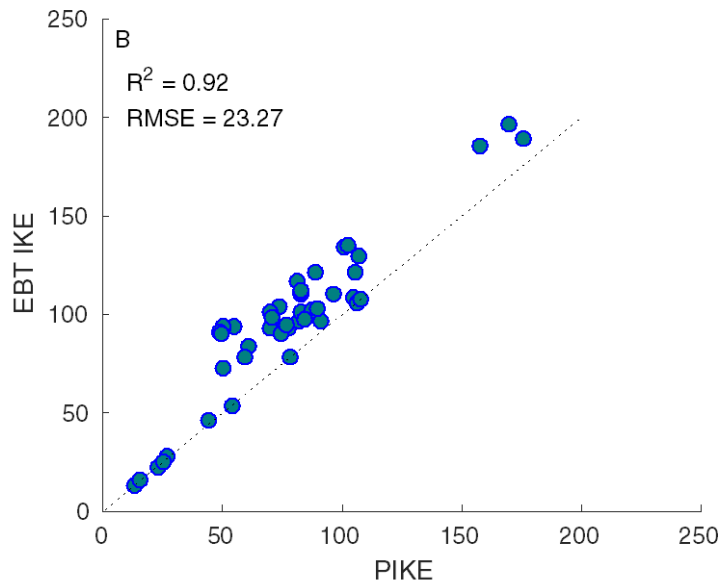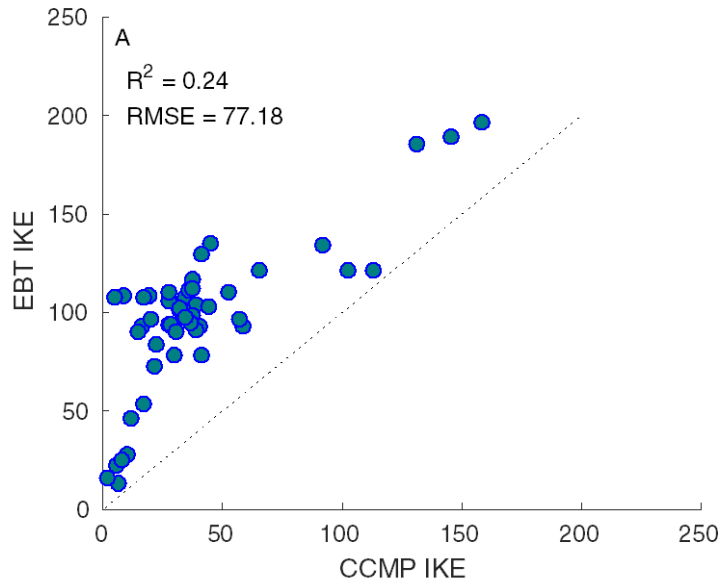
Figure 8: The scatter between EBT IKE (TJ) and a) CCMP IKE (TJ) and b) PIKE (TJ) for fixes that are at or above the 90th percentile of differences between PIKE and EBT IKE. The dotted black line represents y=x line.
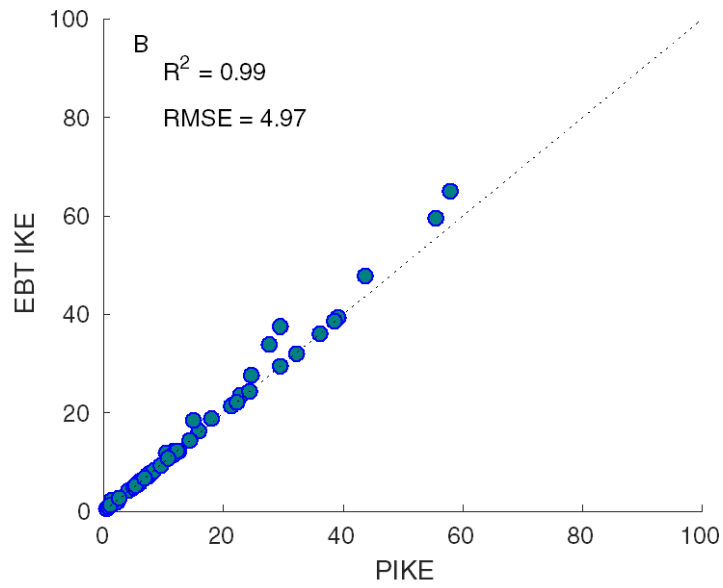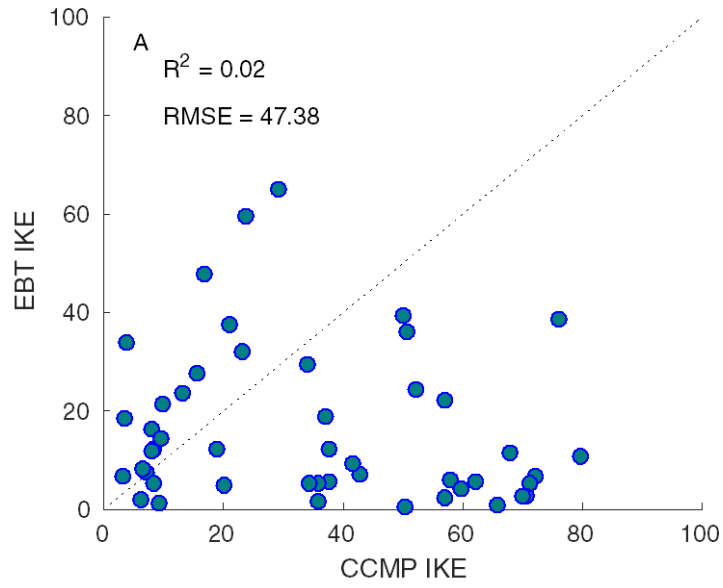
Figure 9: The scatter between EBT IKE (TJ) and a) CCMP IKE (TJ) and b) PIKE (TJ) for fixes that are at or below the 10th percentile of differences between PIKE and EBT IKE. The dotted black line represents y=x line.

figure1.eps

A. EBT IKE_{34-50} vs Resolved CCMP IKE_{34-50}

$R^2 = 0.31$

RMSE = 35.20

EBT IKE_{34-50}

CCMP IKE_{34-50}

B. EBT IKE vs Resolved CCMP IKE_{34-50}

$R^2 = 0.32$

RMSE = 40.46

EBT IKE

CCMP IKE_{34-50}
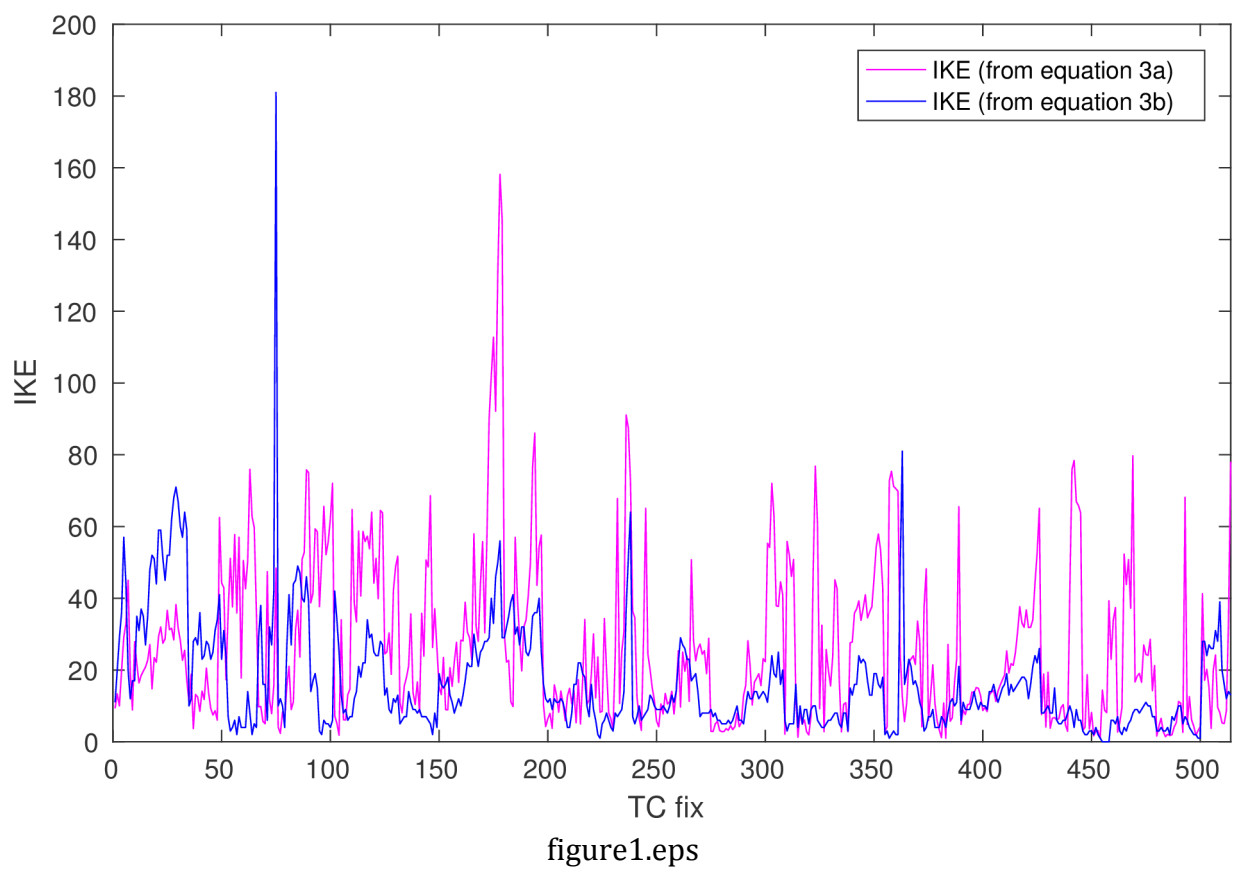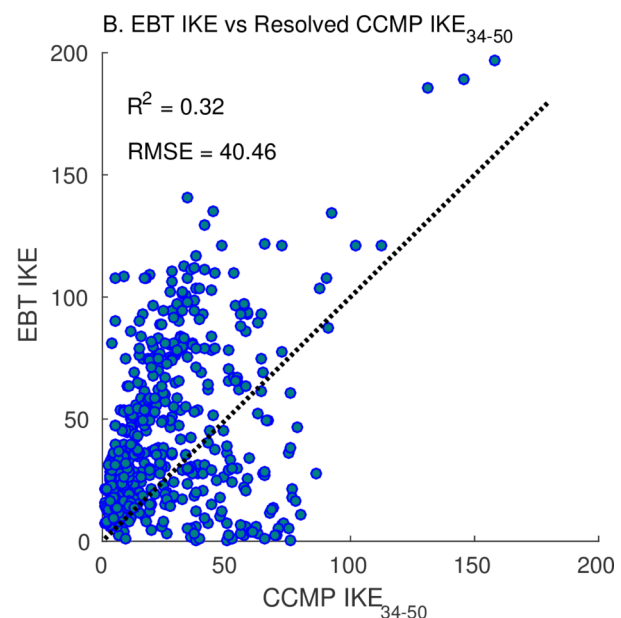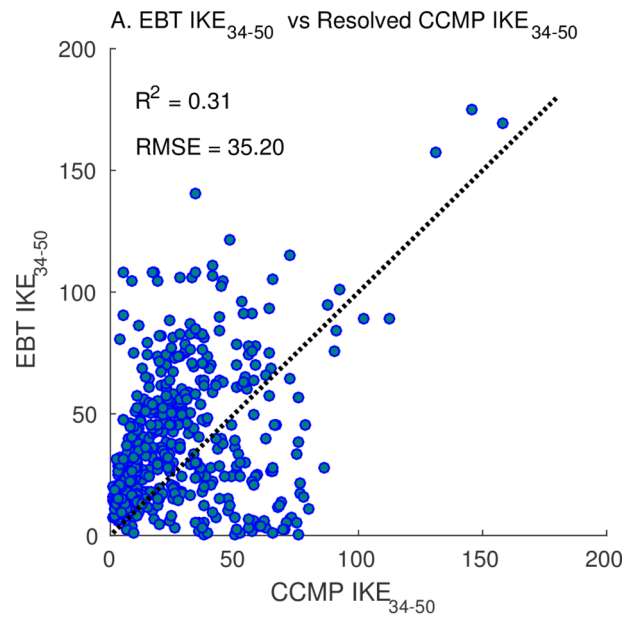
figure2.eps

a   Climatological Seasonal Cycle of IKE_{34-50} (2004-2011)

	June	July	August	September	October	November
EBT IKE 34-50	59	258	579	999	271	113
CCMP IKE 34-50	5	41	123	200	89	47
EBT TCs	6	13	34	44	20	7
CCMP TCs	4	7	15	26	6	5
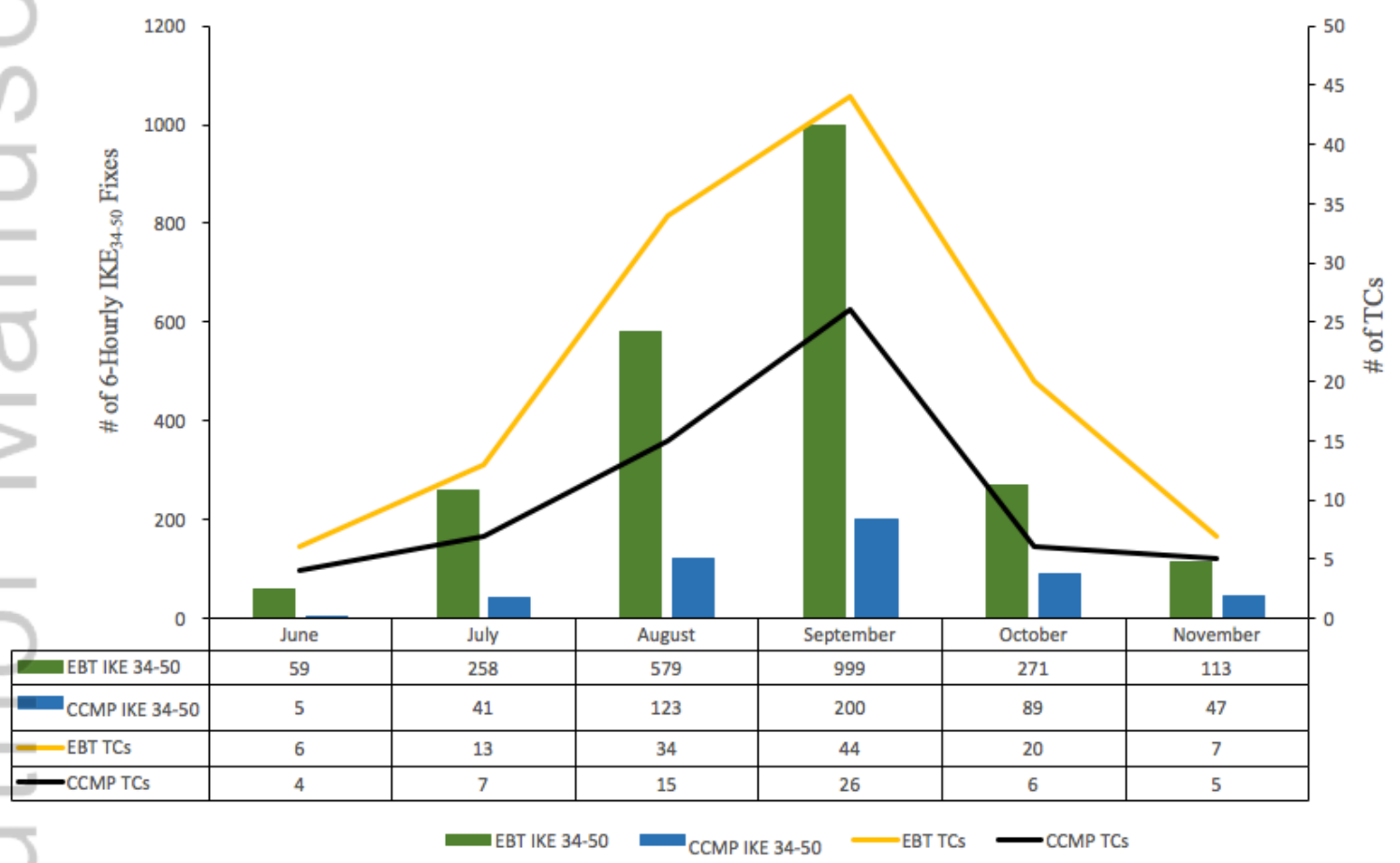
Figure3a.tif

figure3b.eps

(a) EBT IKE34-50

(b) CCMP IKE34-50

(c) a-b

figure4.eps

Figure5.tif

EBT IKE vs PIKE (2004-2011)

A.

$R^2 = 0.45$
RMSE = 35.10

EBT IKE vs PIKE for unresolved CCMP
6-hourly fixes (2004-2011)
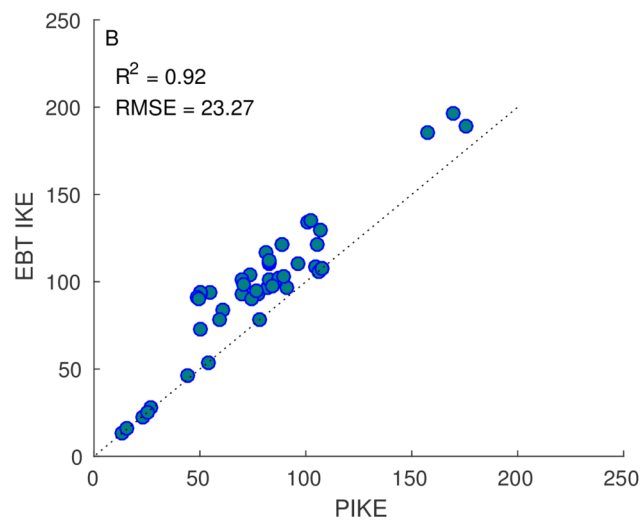
B.

$R^2 = 0.50$
RMSE = 33.41
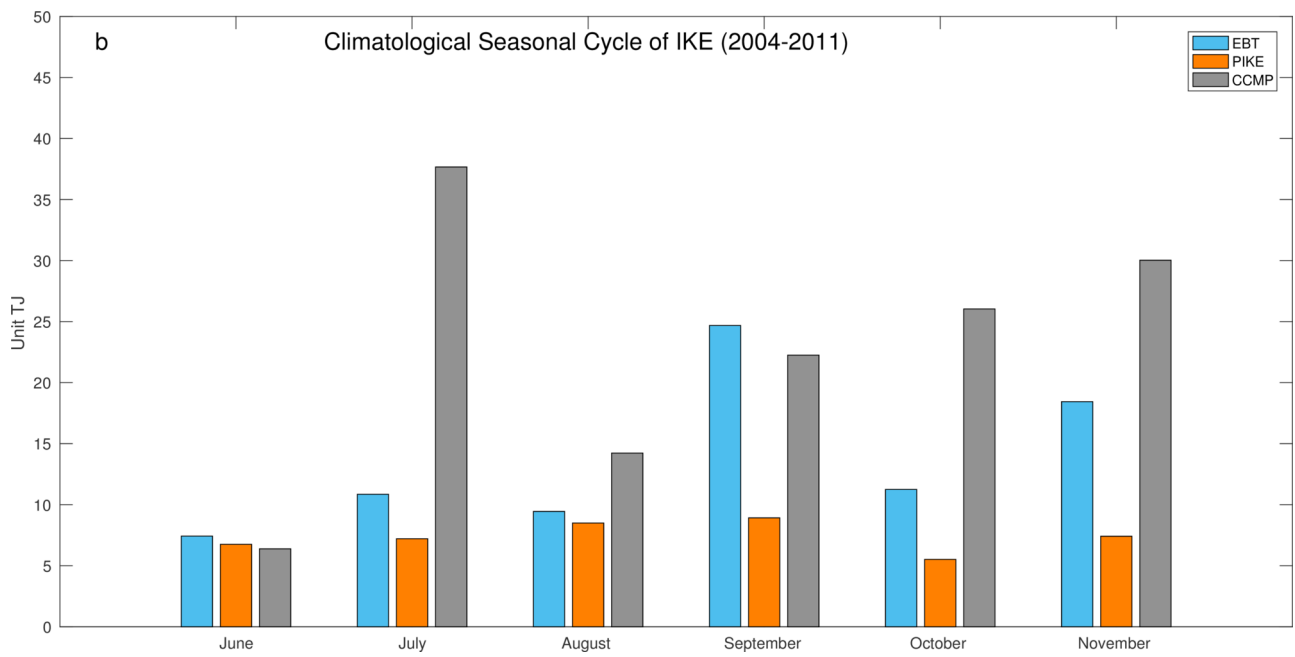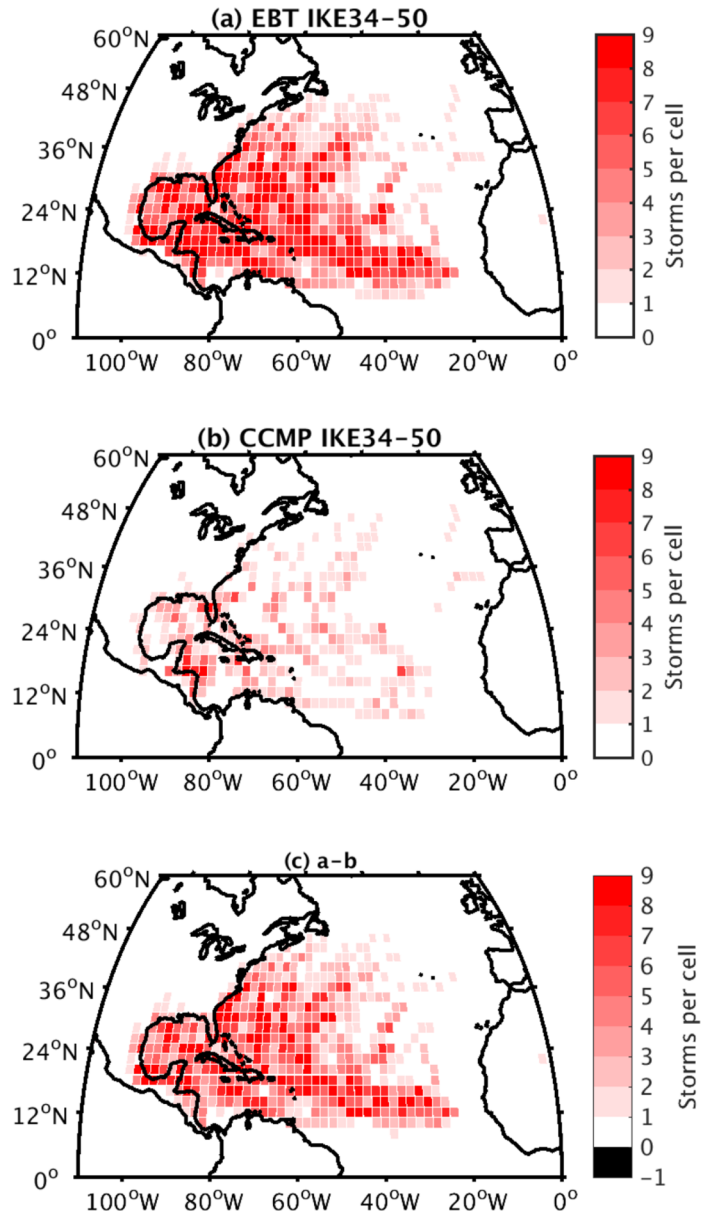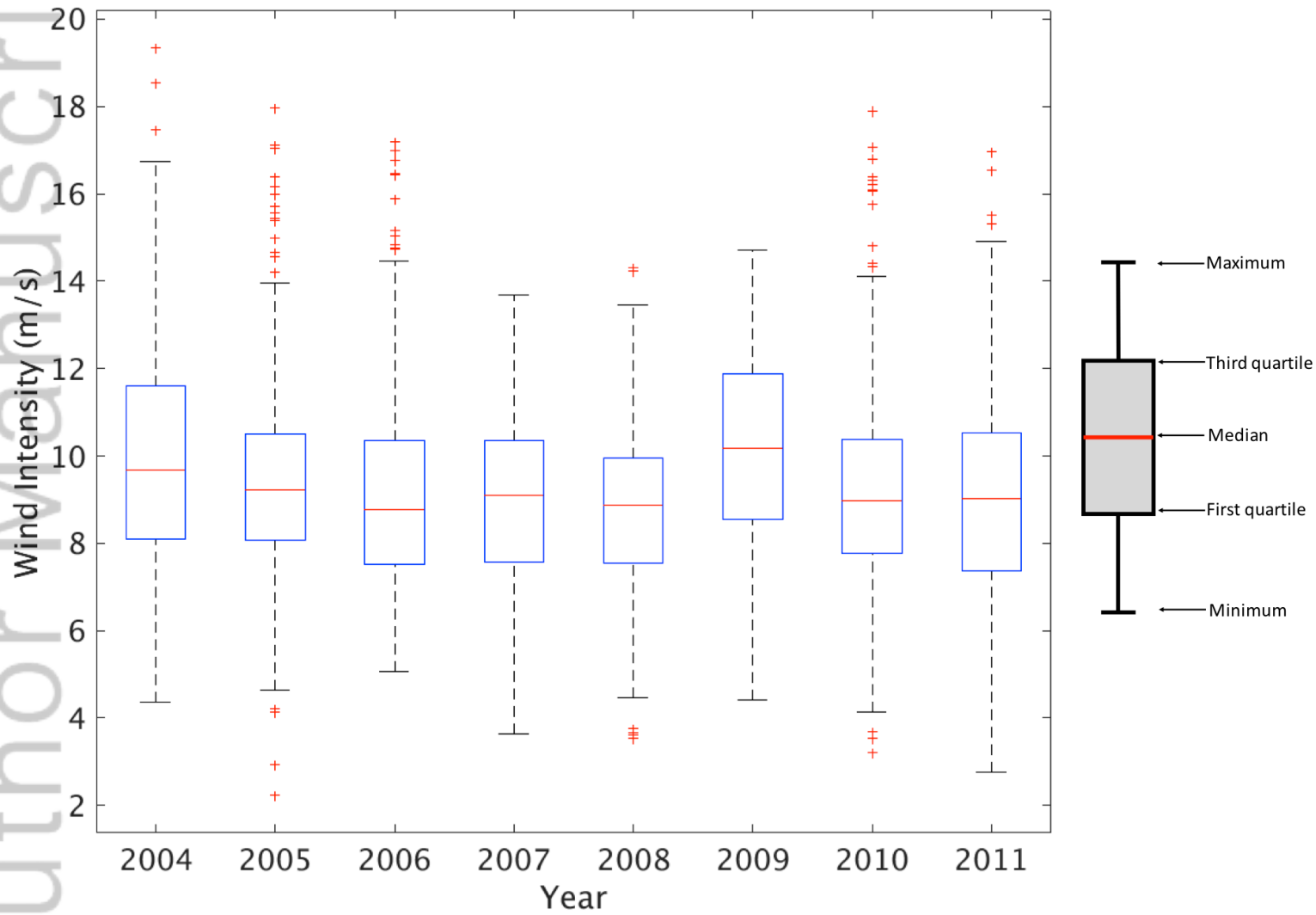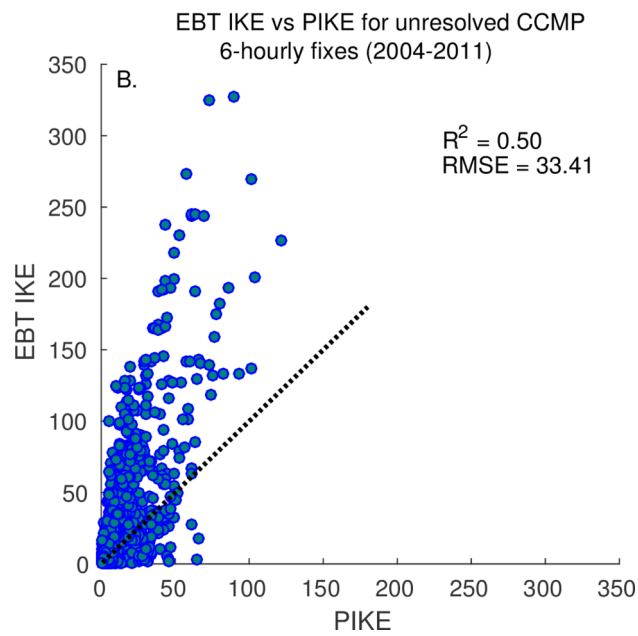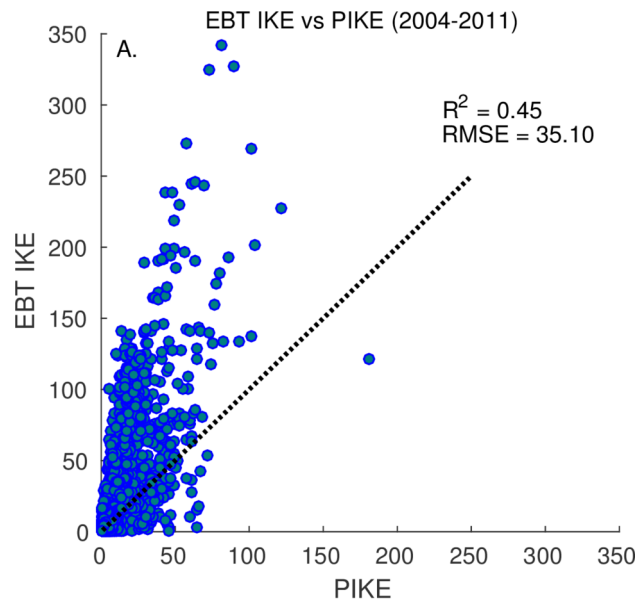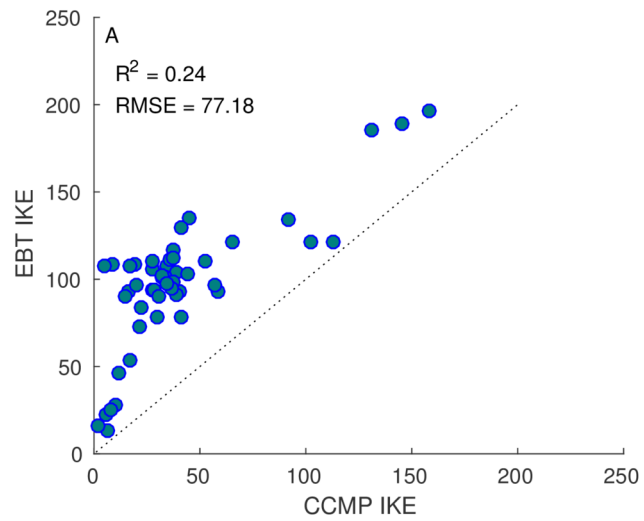
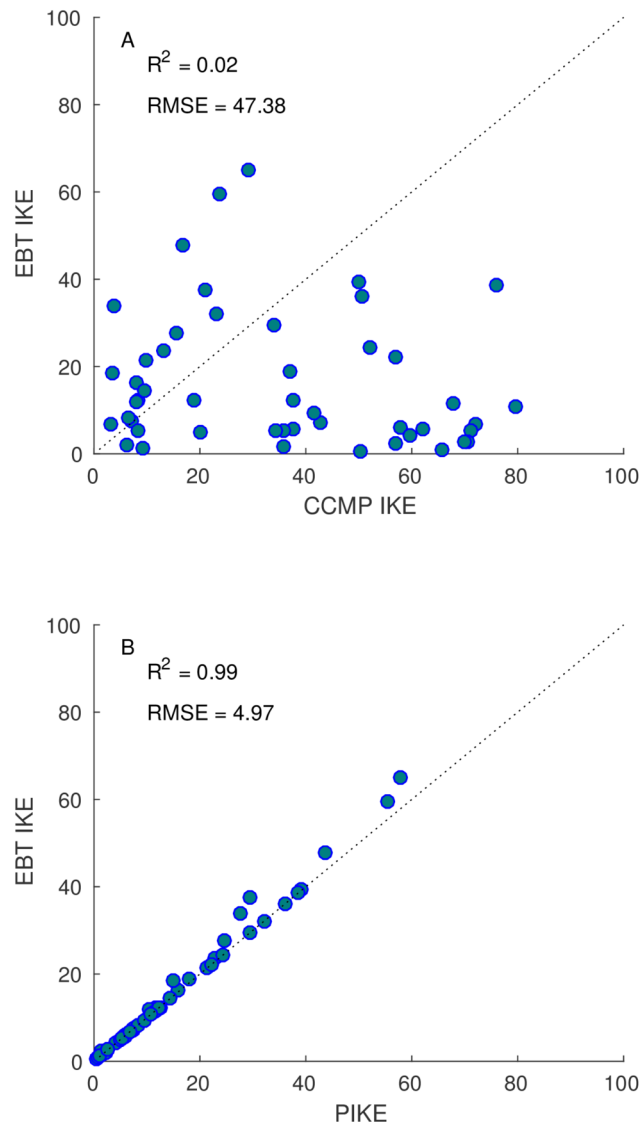figure6.eps
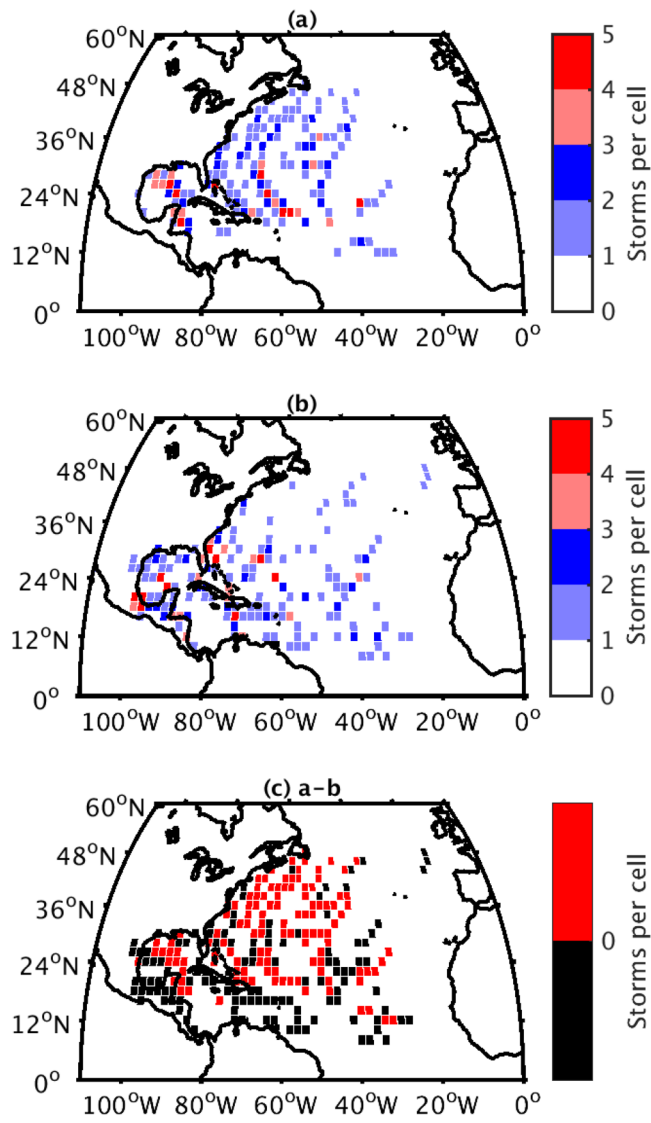
figure7.eps

figure8.eps

figure9.eps

Integrated Kinetic Energy of Atlantic Tropical Cyclones in a Global Ocean Surface Wind Analysis

Sean Buchanan, Vasubandhu Misra[*], and Amit Bhardwaj

* Corresponding Author email: vmisra@fsu.edu

Key findings: The integrated kinetic energy (IKE) of Atlantic tropical cyclones (TCs) is poorly represented in NASA's Cross Calibrated Multi-Platform (CCMP) wind analysis. This bias arises from poor representation of wind structure in large sized TCs and unresolved small TCs. This bias can be improved upon with a proposed proxy IKE that uses kinetic energy of winds at radius of the last closed isobar of the TC.
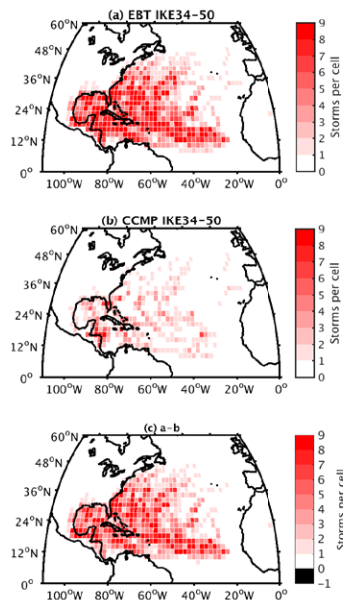
Caption: The composite track density (number of TCs based on non-zero values of 34-50-kt IKE per 2°x2° cell) plot of North Atlantic TCs for the years 2004-2011 from a) EBT, b) CCMP, and c) a-b.